



# Response characteristics of conductance sensor and optimization of control-drive circuit in horizontal pipes

He Li<sup>1</sup> · Yongqiang Cui<sup>1,2</sup> · Jun Li<sup>1,3</sup> · Fengda Zhao<sup>1,2</sup> · Weihang Kong<sup>1,2</sup> · Min Wang<sup>3</sup>

Received: 1 April 2019 / Accepted: 25 June 2019 / Published online: 1 July 2019  
© The Author(s) 2019

## Abstract

Oil–water two-phase flow in horizontal oil-producing wells with low velocity and high water cut generally presents the phenomenon that the underlayer shows water flow and the upperlayer presents oil flow or a dispersion of oil in water flow. And existing ring-shaped conductance water cut meter cannot obtain the online and real-time response values corresponding to oil field water conductivity in the calculating water holdup procedure. To tackle this issue, this paper designs a mini-conductance probe array (MCPA). In order to further investigate the ability of the total flow rate of the allowable measurement fluid and the parameters valuing of the water cut in horizontal segregated flow, this paper also analyzes the performance of MCPA with different structure parameters in terms of the spatial sensitivity distribution characteristics. Firstly, the geometry model and mathematical model of MCPA are designed, and the MCPA simulation model is analyzed by using the finite element method. Then, the optimum structure parameter results of the sensors are obtained through analyzing the spatial sensitivity distribution characteristics of MCPA in consideration of different distance between the two electrodes and different inner diameters. Lastly, the MCPA different parameters are developed, and experiments are carried out in horizontal multiphase flow experiment facility to analyze spatial sensitivity distribution characteristics of MCPA with different inner diameters on the basis of optimum parameters. Experimental results demonstrated that MCPA with a larger inner diameter would have high measurement accuracy in variation range of water cut, and has a high adaptability in horizontal oil-producing wells with relatively high flow rate and different flow conditions.

**Keywords** Horizontal oil–water two-phase flow · Segregated flow · Mini-conductance probe array · Control-drive circuit · Water holdup

## Introduction

Horizontal two-phase flow is widespread in the petroleum industry, chemical engineering, pharmacy and nuclear reaction, etc. In particular, with the rapid development of horizontal well technology, the accurate measurements for the phase volume fraction (liquid holdup) and production rate of each component at any production layer in oil–water

two-phase flow are very significant for the oil development and the oil production optimization (Li et al. 2016). In particular, the water cut of the whole oil-producing well would increase sharply when the partial well sections are flooded in the process of horizontal well production and development. And it would have a negative impact on development effectiveness of horizontal oil-producing wells, and even cause the disuse of oil-producing wells (Zhai et al. 2012a, b; Kong et al. 2015). Hence in order to improve the horizontal oil field logging techniques and optimize the oil production, horizontal production profile logging data interpretation is becoming an important research hotspot in the related research fields. Consequently, water cut, as an important and representative indicator, needs to be acquired as accurate as possible (Li et al. 2016; Feng et al. 2018).

In the investigations on the flow patterns of horizontal oil–water two-phase flow patterns, experimental and theoretical study in a horizontal pipe with the inner diameter

✉ Weihang Kong  
whkong@ysu.edu.cn

<sup>1</sup> School of Information Science and Engineering, Yanshan University, Qinhuangdao 066004, China

<sup>2</sup> Key Laboratory for Computer Virtual Technology and System Integration of Hebei Province, Qinhuangdao 066004, Hebei, China

<sup>3</sup> Logging and Testing Services Company, Daqing Oilfield Limited Company, Daqing 163453, China

of 50.1 mm was comprehensively performed by Trallero et al. (1996), and then the flow patterns are classified into segregated flow and dispersed flow; an experiment on the flow patterns under oil–water two-phase conditions in a large inner diameter horizontal pipe was conducted by Yang et al. (2008), and the same result of flow patterns classification is obtained. Hence, in the actual horizontal oil wells with long distance undulating, a mixed flow pattern, which is mainly horizontal segregated flow, whose phenomenon that the underlayer shows a water flow and the upperlayer shows an oil flow or a dispersion of oil in water, exists in the horizontal oil–water two-phase flow with low velocity and high water cut, compared to vertical wells, and flow pattern and velocity are greatly influenced by the inclination of horizontal oil-producing wells (Trallero et al. 1996; Lum et al. 2006); so the most previous profile parameters measurement instruments for the production of vertical wells cannot be directly used for horizontal oil-producing wells (Guo et al. 2009). And it can be deduced that the various complicated flow structures in horizontal oil–water two-phase flows raise many challenges in the profile parameter measuring sensor design.

The conductance sensor with special structure and characteristic is applicable to more complex environmental conditions and different fields (Asali et al. 1985; Wang et al. 2016). In particular, the ring-shaped electrodes conductance sensor has almost no disturbance to fluid and then could be widely used in vertical upward two-phase flow (Lucas et al. 2000; Devia and Fossa 2003; Jin et al. 2008; Shi et al. 2010). The measurement principle of the conductance sensor indicates that water cut can be determined by oil–water mixture conductivity and water conductivity. In horizontal oil-producing wells, the response values corresponding to the oil–water mixture conductivity could be measured online in the process of fluid flowing by using the ring-shaped conductance probe (RSCP) (Zhai et al. 2012a, b). However, due to the structure characteristics of the horizontal oil-producing wells and structure limitations of the ring-shaped conductance water cut meter (RSCWCM), the electrodes of RSCP must still be immersed in the oil–water segregated flow in whole sampling procedure so that the online and real-time response values corresponding to the oil field water conductivity of horizontal oil-producing wells cannot be obtained (Oddie and Pearson 2004; Shi et al. 2010). In addition, the fluid temperature and mineralization degree in horizontal oil-producing wells are very different from those in the simulation wells (Johansen and Jackson 2000; Sætre et al. 2010); as a result, the water phase calibration results of the simulation experimental facility cannot be used to calculate the water holdup directly in horizontal oil-producing wells in general (Shi et al. 2010; Kong et al. 2016a). Consequently, the previous RSCWCM cannot be applied in horizontal oil-producing wells for the reason that

it cannot obtain the online and real-time the response values corresponding to the oil field water conductivity.

Considering that the values of the structure parameters would influence the uniformity of the spatial sensitivity directly, this paper analyzes and discusses the characteristics of the spatial sensitivity in the measurement field of MCPA from the aspects of the different electrodes separations and different inner diameters of the insulated flow pipe and ability of the allowable total flow rate of the fluid and the values of the water holdup parameters in the condition of horizontal segregated flow, on the basis of the conductance sensor for water conductivity measurement in horizontal oil–water two-phase flow (Kong et al. 2016b, 2017). Then, the response characteristics of water conductivity measurement of MCPA with different inner diameters are analyzed by the simulation experiments and simulation wells experiments in horizontal oil water two-phase flow on the foundation of the structure parameter optimization.

## Model and simulation of MCPA

### Geometry model

Figure 1 shows the geometry of MCPA. MCPA consists of six pairs of metal parallel electrodes, in which each pair of metal parallel electrodes is a mini-conductance probe (MCP), and serves as the exciting electrode and the measuring electrode along the axial direction. In addition, one end of each electrode is flush-mounted on the inside wall of the insulated flow pipe, six electrodes represented by  $E_1$  to  $E_6$  are homogeneously distributed on the same upstream cross section along the axial direction, and six electrodes represented by  $M_1$  to  $M_6$  are homogeneously distributed on the same downstream cross section along the axial direction. Each pair of  $E_i$  and  $M_i$  electrodes forms the  $i$ th mini-conductance probe (MCP <sub>$i$</sub> ), where  $i$  ranges from 1 to 6. MCP <sub>$i$</sub>  is located at different locations in the space of the insulated flow pipe, where MCP<sub>1</sub> is located at the bottom of the insulated flow pipe, MCP<sub>4</sub> is located at the top of the insulated flow pipe, MCP<sub>2</sub> and MCP<sub>6</sub> are located at the same height of

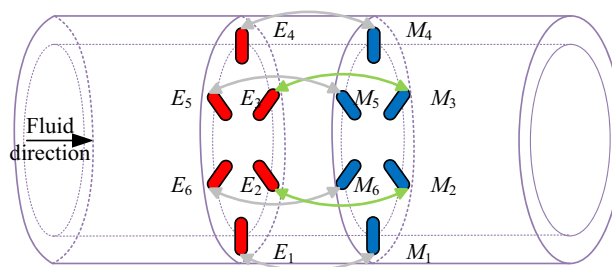


Fig. 1 Sketch of MCPA geometry model

the insulated flow pipe,  $MCP_3$  and  $MCP_5$  are located at the same height of the insulated flow pipe.

The representative structure parameters and the coordinates of MCPA are shown in Fig. 2, in which  $S$  is the distance between two electrodes of  $MCP_i$ ,  $d$  is the diameter of each metal parallel electrode,  $h$  is the measurement field height of the metal parallel electrode,  $D$  is the inner diameter of the insulated flow pipe,  $D_w$  is the thickness of the insulated flow pipe, and  $L$  is the axial length of the insulated flow pipe.

### Mathematical model

In order to reduce or inhibit the leakage current in the flow field, the design of MCPA system drive circuit introduced the real ground (the earth or shell of instrument) and imaginary ground, that is, the sensor electrode excitation is carried out by the digital ground power supply  $u_{\text{digit}}$  and the sensor output signal used analog power supply  $u_{\text{ground}}$  for different amplifiers, since the voltage reference point  $u_{\text{ground}}$  of the excited part and the  $u_{\text{digit}}$  of the measured part are isolated from each other, which means that corresponding to real ground  $u_{\text{ground}} = 0$  as the shell of instrument, the measurement pipes internal fluid of MCPA have independent electric field and electric potential, which also has digital ground  $u_{\text{digit}} = 0$  as the reference point.

Since the measurement field of MCPA is much smaller than the wavelength of the electric field, the electric field of MCPA can be considered as quasi-stationary electric field, which can be described with the theory of the static electric field, that is, meeting the Laplace equation with some certain boundary conditions under the cylindrical coordinates (Yang et al. 2008; Zhai et al. 2012a, b):

$$\nabla^2 u_{\text{digit}}(r, \varphi, z) = \frac{1}{r} \frac{\partial}{\partial r} \left( r \frac{\partial u_{\text{digit}}}{\partial r} \right) + \frac{1}{r^2} \frac{\partial^2 u_{\text{digit}}}{\partial \varphi^2} + \frac{\partial^2 u_{\text{digit}}}{\partial z^2} = 0 \tag{1}$$

and each  $MCP_i$  of MCPA is constrained by the essential boundary conditions, which can be expressed as:

$$u_{\text{digit}} = 0, \quad \left( r \in \left[ \frac{D}{2} - h, \frac{D}{2} \right], \varphi \in \left[ \frac{i-1}{3} \pi - \arctan\left(\frac{d}{D-2h}\right), \frac{i-1}{3} \pi + \arctan\left(\frac{d}{D-2h}\right) \right], \frac{S-d}{2} \leq z \leq \frac{S+d}{2} \right) \tag{2a}$$

$$\frac{\partial u_{\text{digit}}}{\partial r} = \frac{I_e}{S_d}, \quad \left( r \in \left[ \frac{D}{2} - h, \frac{D}{2} \right], \varphi \in \left[ \frac{i-1}{3} \pi - \arctan\left(\frac{d}{D-2h}\right), \frac{i-1}{3} \pi + \arctan\left(\frac{d}{D-2h}\right) \right], -\frac{S+d}{2} \leq z \leq -\frac{S-d}{2} \right) \tag{2b}$$

$$\frac{\partial u_{\text{digit}}}{\partial z} = 0, \quad \left( z = \pm \frac{L}{2} \right) \tag{2c}$$

where  $u_{\text{digit}}$  is the internal electric potential distribution of MCPA,  $I_e$  represents the direct current applied to exciting electrodes,  $D$  is the ID of the insulated flow pipe,  $L$  is the axial length of the insulated flow pipe, and  $S_d$  is the surface area of the electrodes of  $MCP_i$ .

### Simulation analysis for electric field

The finite element simulation was employed to analyze the distribution characteristics of the inner electric field of MCPA. Figure 3 shows the three-dimensional simulation

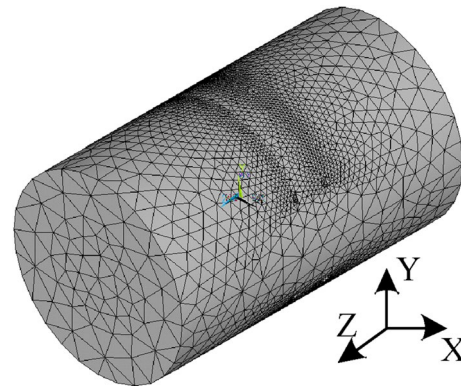
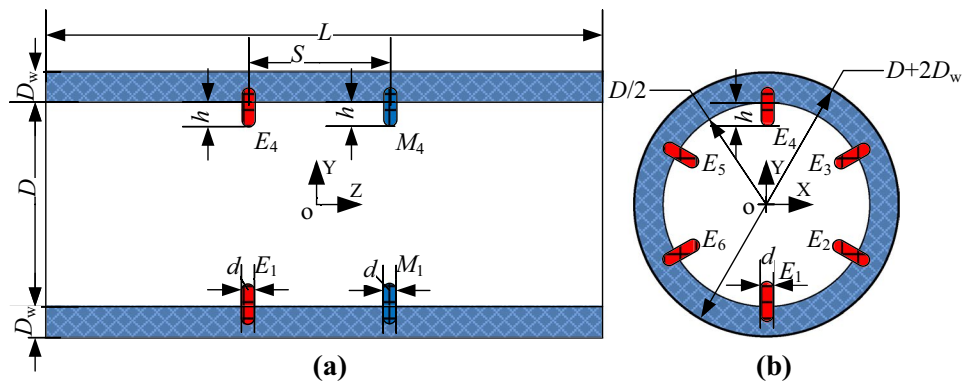


Fig. 3 3D meshed model of MCPA with 164,810 grids,  $L=0.05$  m,  $D=0.03$  m,  $h=0.002$  m,  $d=0.0015$  m,  $S=0.005$  m and  $\sigma_w = 100 \mu\text{S/cm}$

Fig. 2 Sketches of structure parameters and coordinates of MCPA: a axial section; b cross section



model established by SOLID232 of ANSYS software, which uses the free meshing as the grid type. The free meshing has strong adaptability and can adapt to the curved surfaces and curves with large variation in curvature especially. Although the grid number of models divided automatically by free meshing is not the same exactly, it only has a slight influence on the simulation result and can be ignored. Then, the simulation way has a nice repeatability and thus the free meshing is used as the grid type. The total grid number of the units of the meshed finite model is 164 810, the structure parameters of MCPA are set as follows:  $L=0.05$  m,  $D=0.03$  m,  $h=0.002$  m,  $d=0.0015$  m and  $S=0.005$  m,

The sectional views of the electric field distribution of MCPA are shown in Fig. 4. Figure 4a shows the electric field distributions of  $MCP_1$  and  $MCP_4$  in the YoZ cross section of MCPA. Analyzed from Fig. 4a, the electric field is relatively strong around the two electrodes of  $MCP_1$  and  $MCP_4$ , respectively, and the electric field in the area far from the electrodes is relatively weak, toward the value of zero. And the top  $MCP_4$  and the bottom  $MCP_1$  in the YoZ cross section generate a relatively strong local electric field, which is relatively independent and non-interference. Figure 4b shows the electric field distributions of  $MCP_1$  in the XoZ cross section of MCPA. In the XoZ section, there exists a relatively strong local electric field around the two electrodes of  $MCP_1$ , and the local electric field far from the electrodes is relatively weak, even to 0. Figure 4c shows the electric field distributions of the  $MCP_i$  in the XoY section of MCPA. In Fig. 4c, the six separate local electric fields are distributed uniform at the different positions of the XoY cross section, and independent of each other.

## Analysis on the spatial sensitivity of MCPA

Sensitivity characteristics are important performance indicators of conductance sensor. When conducting the oil–water two-phase flow measurement under the downhole, to reduce the impact of flow patterns, the conductance sensor is

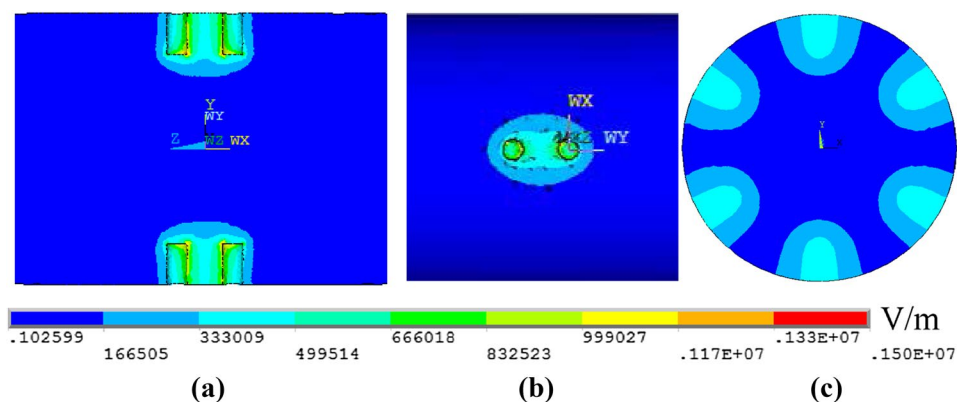
needed to be designed as sensitivity uniformly distributed (Gao et al. 2010). This paper processed the normalization on the parameter  $H$ , which is  $Y$ -axis location of the center of mass of the insulated oil droplet (the diameter is 2 mm) in the sensitive space of the MCPA whose inner diameter is  $D$ , the result of which can be expressed as  $H/D$ . And the  $H/D$  ranges from  $1/D$  to  $1 - 1/D$ . Then, the finite element model can be solved by changing the location  $(x, H/D, z)$  of the center of mass of the insulated oil droplet in the sensitive space. And then, the distribution characteristic of the spatial sensitivity can be obtained.

Taking into account that the parameter  $S$  is one of the main factors influencing the uniformity of the sensitivity field distribution in MCPA measurement field and that parameter  $D$  can determine the stability of the water conductivity measurement in certain horizontal segregated flow with size-fixed flow rate and water cut, the structure parameters were optimized using different  $h$  values under the condition that  $D=20$  mm in the early work, and the optimum structure parameters of different  $h$  values can be obtained using the uniformity of both the electric field and the spatial sensitivity. Hence, the effect of different values of the parameters  $S$  and  $D$  on the spatial sensitivity distribution characteristics of MCPA was discussed, taking  $MCP_1$ , composed of the  $E_1$  and  $M_1$  at the bottom of the insulated flow pipe, as the example, when  $h=2$  mm,  $d=1.5$  mm and the oil conductivity  $\sigma_o$  is  $10^{-9}$   $\mu\text{S/cm}$ .

## The effect of different values of parameter $S$

Specifying  $D=20$  mm, the spatial sensitivity characteristics of  $MCP_1$  measurement area are further discussed and analyzed in three different conditions that parameter  $S$  is set to 4 mm, 5 mm and 6 mm, respectively. Figure 5 shows the spatial sensitivity distribution characteristics in the YoZ plane, along the  $Z$ -axis direction and along the  $Y$ -axis direction, under different  $S$  values. It can be known from the spatial sensitivity distribution in the YoZ plane that a large difference exists at the different locations in the YoZ plane under

**Fig. 4** Sectional views of the electric field distribution of MCPA: **a** YoZ plane sectional view; **b** XoZ plane sectional view; **c** XoY plane sectional view





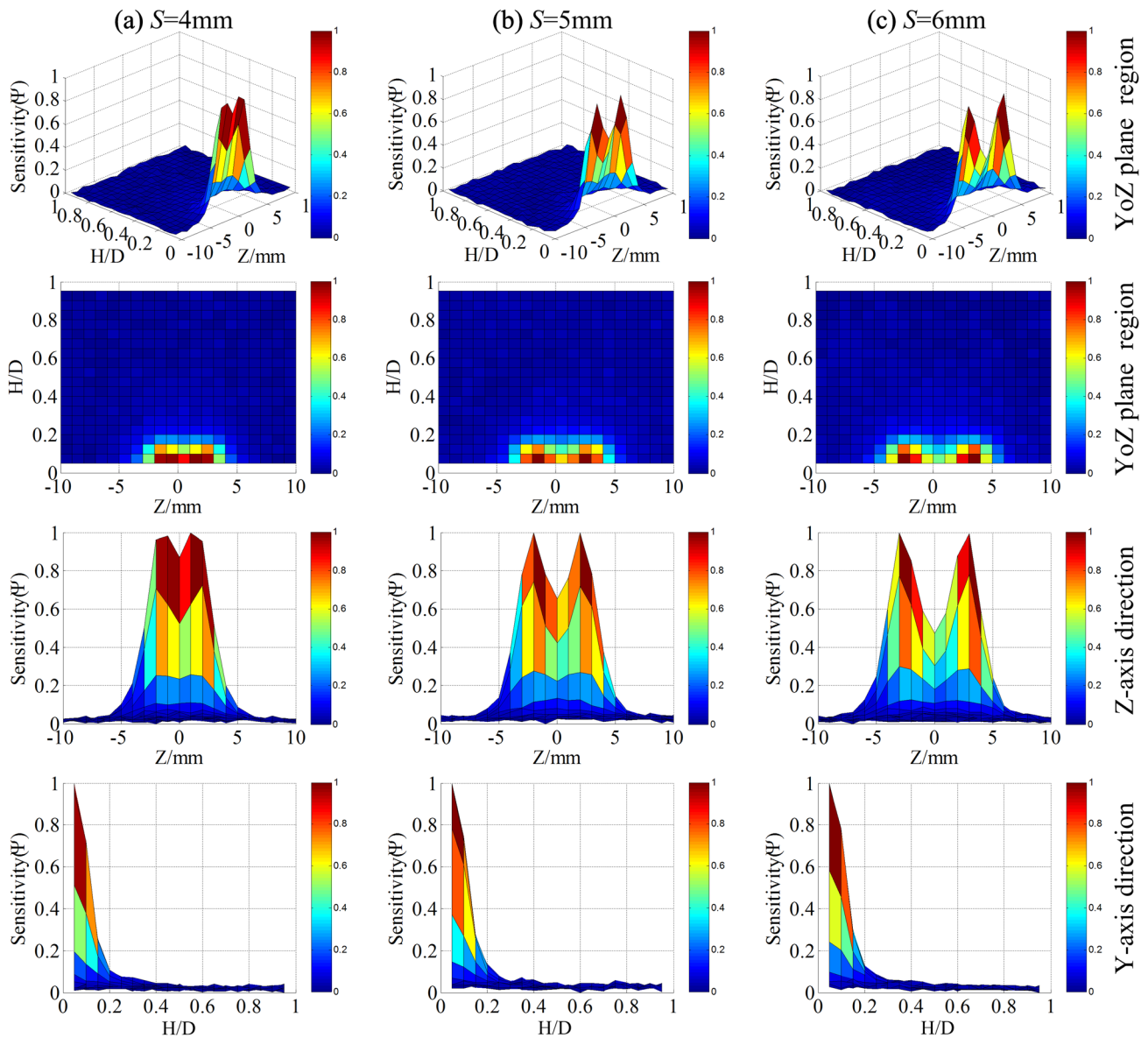


**Fig. 5** Distribution maps of spatial sensitivity of  $MCP_1$  under three different  $S$  values:  $D=20$  mm,  $h=2$  mm and  $d=1.5$  mm

the different  $S$  values and the spatial sensitivity in the vicinity of measurement field is relatively high, and the spatial sensitivity away from the electrodes is relatively low and tends to be 0. And it can be analyzed from the  $Z$ -axis direction that the spatial sensitivity distribution of  $MCP_1$  along the  $Z$ -axis direction is greatly influenced by the parameter  $S$  and with the parameter  $S$  increases, the uniformity of the spatial sensitivity distribution reduces in the measurement field between the two electrodes of  $MCP_1$ . So the spatial sensitivity distribution is more uniform when  $S=4$  mm. It can be analyzed from the  $Y$ -axis direction that the spatial sensitivity distributions of  $MCP_1$  are basically consistent at different locations along the  $Y$ -axis direction. And with the increase in the  $H/D$ , the spatial sensitivity under different

$S$  values gets smaller, especially falls at a high rate and demonstrates high gradient descent in the interval  $(1/20, 6/20)$  and shows a slow change of the spatial sensitivity and tends to be 0 in the interval  $(6/20, 19/20)$ .

To further discuss the influence of different  $S$  values on the spatial sensitivity distribution characteristic in the condition of the insulated flow pipe with  $D=20$  mm, the results of the sensitivity distribution curves along the  $Y$ -axis at the location that  $z=0$  under different  $S$  values are shown in Fig. 6. It can be known that with the increase in  $H/D$ , the values of the spatial sensitivity under different  $S$  values show a decreasing tendency, and the sensitivity distribution curve firstly tends to be the minimum value when  $S=4$  mm. Simultaneously, the spatial sensitivity of  $MCP_1$  is large, falls

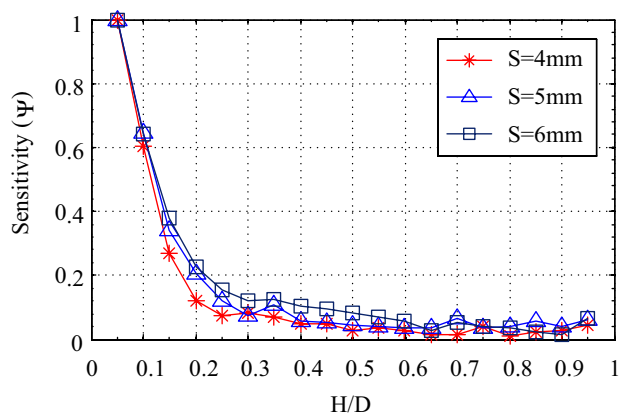


**Fig. 6** Sensitivity distribution curves of MCP<sub>1</sub> under three different  $S$  values at  $z=0$ :  $D=20$  mm,  $h=2$  mm and  $d=1.5$  mm

fast, and demonstrates a high gradient, which shows that the measurement signals of MCP<sub>1</sub> are greatly influenced by the oil droplet when  $H/D$  is located in the  $(1/20, 6/20)$ ; the sensitivity changes slowly and tends to be the minimum value when  $H/D$  is located in the  $(6/20, 19/20)$ , which shows that the measurement signals of MCP<sub>1</sub> are almost not influenced by the oil droplet and even never influenced in the interval.

From the above analysis, the spatial sensitivity distribution of MCP<sub>1</sub> is more uniform when  $S=4$  mm in the condition of the insulated flow pipe with  $D=20$  mm. And the sensitivity distribution of MCP<sub>1</sub> along the  $Y$ -axis is gently influenced by the parameter  $S$  and the measurement signals of MCP<sub>1</sub> are slightly or even not influenced by the insulated oil droplet or the non-conductive materials in the interval of  $H/D \in (6/20, 19/20)$ . Hence, in that condition, a more reliable water phase calibration value can be obtained.

### The effect of different values of parameter $D$

The parameter  $S$  after optimization is 4 mm when  $D=20$  mm,  $h=2$  mm,  $d=1.5$  mm. Hence, the effect of parameter  $D$  valued 20 mm, 30 mm, 40 mm, 50 mm, 60 mm and 70 mm was analyzed and discussed, respectively, on the spatial sensitivity of MCP<sub>1</sub> in the measurement field under the condition of certain values of the parameters  $h$ ,  $d$  and  $S$ . Figure 7 shows the spatial sensitivity distribution characteristics of MCP<sub>1</sub> in the  $YoZ$  plane, along the  $Z$ -axis direction and along the  $Y$ -axis direction, under different  $D$  values. It can be known from the sensitivity distribution in the  $YoZ$  plane that the sensitivity distributions in the  $YoZ$  plane under six different  $D$  values are basically consistent which shows a large difference in the spatial sensitivity in the measurement field. The spatial sensitivity in the vicinity of the measurement field between the two electrodes is higher and that away from the measurement field is lower and tends to be 0. It can be known from the

spatial sensitivity distribution along the  $Z$ -axis that the spatial sensitivity distributions along the  $Z$ -axis under six different  $D$  values are basically consistent which is hardly influenced by the parameter  $D$  and that the spatial sensitivity in the vicinity of the two electrodes is more uniform. It can be known from the sensitivity distribution along the  $Y$ -axis that the sensitivity distributions along the  $Y$ -axis under six different  $D$  values are basically consistent which shows a decreasing tendency and that the spatial sensitivity under six different  $D$  values is higher, changes fast and has a great gradient descent in the interval of  $(1/20, 6/20)$ ,  $(1/30, 6/30)$ ,  $(1/40, 6/40)$ ,  $(1/50, 6/50)$ ,  $(1/60, 6/60)$  and  $(1/70, 6/70)$ , respectively. And it can be also known that the spatial sensitivity in the interval of  $(6/20, 19/20)$ ,  $(6/30, 29/30)$ ,  $(6/40, 39/40)$ ,  $(6/50, 49/50)$ ,  $(6/60, 59/60)$  and  $(6/70, 69/70)$  is lower and tends to be 0.

To further investigate the effect of the six different  $D$  values on the spatial sensitivity characteristic of MCP<sub>1</sub>, the curves of the spatial sensitivity distribution with six different  $D$  values along the  $Y$ -axis at the position that  $z=0$  are shown in Fig. 8. It can be seen from the curves that with the increase in the  $H/D$ , the spatial sensitivity distribution of MCP<sub>1</sub> with six different  $D$  values along the  $Y$ -axis shows a decreasing tendency and simultaneously the spatial sensitivity under six different  $D$  values is higher, changes fast and has a great gradient descent in the interval of  $(1/20, 6/20)$ ,  $(1/30, 6/30)$ ,  $(1/40, 6/40)$ ,  $(1/50, 6/50)$ ,  $(1/60, 6/60)$  and  $(1/70, 6/70)$ , respectively, which shows MCP<sub>1</sub> is greatly influenced by the insulated oil droplet in the measurement field. And it can be also known that the spatial sensitivity changes slowly and tends to be 0 when the  $H/D$  is in the interval of  $(6/20, 19/20)$ ,  $(6/30, 29/30)$ ,  $(6/40, 39/40)$ ,  $(6/50, 49/50)$ ,  $(6/60, 59/60)$  and  $(7/70, 69/70)$  which shows that the spatial sensitivity of MCP<sub>1</sub> is slightly influenced by the insulated oil droplet in the measurement field.

From the above analysis, the spatial sensitivity distributions corresponding to the six different  $D$  values of the insulated flow pipe in the  $YoZ$  plane and that along the  $Z$ -axis are basically consistent. It can be analyzed that the variation range of the spatial sensitivity of MCP<sub>1</sub> with six different  $D$  values of the insulated flow pipe when  $H/D \in (1 \text{ mm}/D, 6 \text{ mm}/D)$  is from 1 to 0.1, falls fast and show a large gradient descent and that when  $H/D \in (6 \text{ mm}/D, (D-1) \text{ mm}/D)$  changes slowly and tends to be 0. Consequently, in the condition with six different  $D$  values of the insulated flow pipe, the influence on the actual measurement signals of MCP<sub>1</sub> from the insulated oil droplet and non-conductive materials is small and tends to be 0, where the reliable water conductivity measurement signals can be obtained.

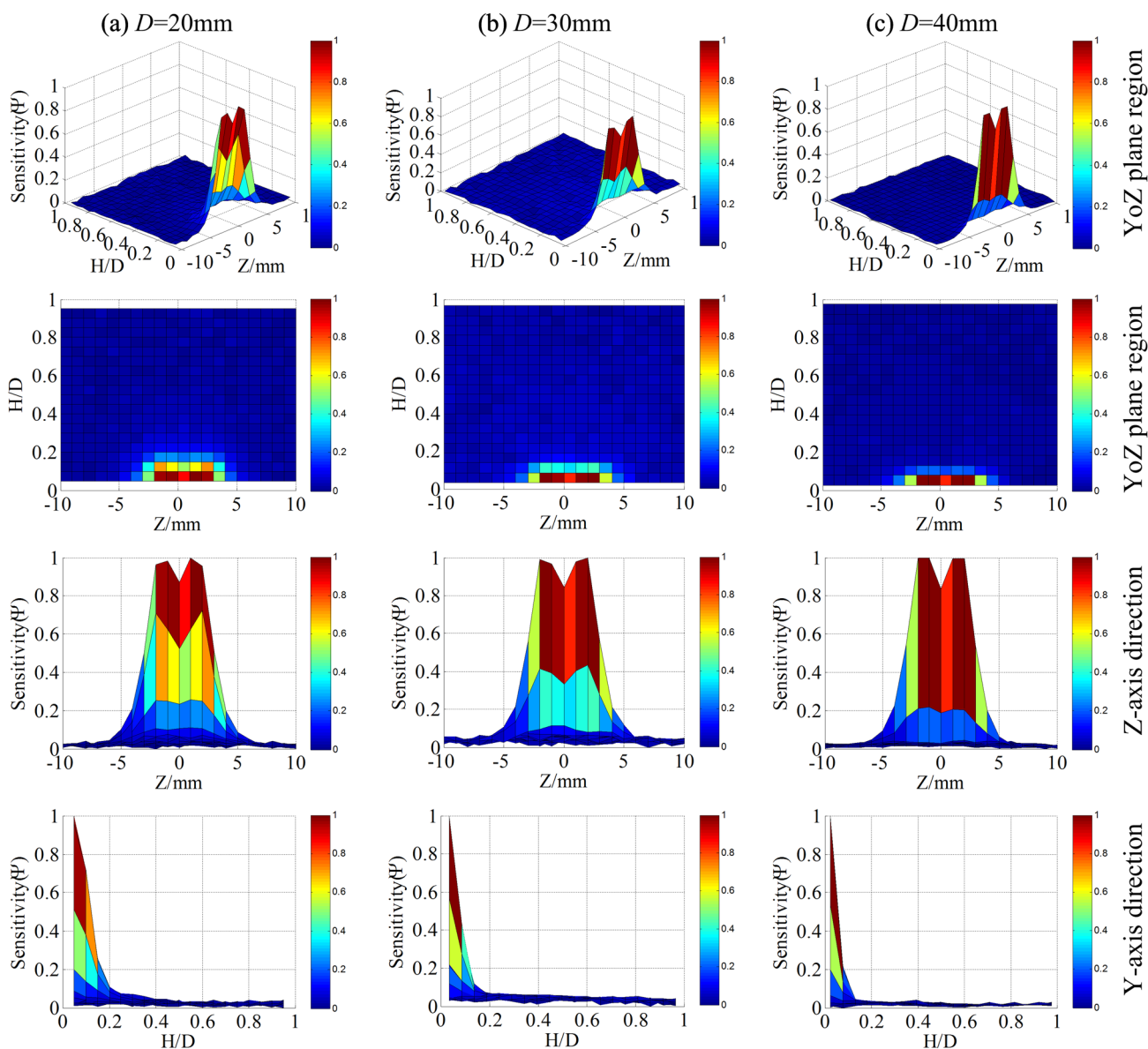


Fig. 7 Distribution maps of spatial sensitivity of  $MCP_1$  under six different  $D$  values:  $h=2$  mm,  $d=1.5$  mm and  $S=4$  mm

### Analysis of experiment results in horizontal oil water two-phase flow

On the above basis of the analyzed spatial sensitivity characteristics of the sensors with different structure parameters, the response characteristics of MCPA with three different  $D$  values in horizontal oil–water flow were analyzed by the simulation well experiment, where the structure parameters after the optimization of MCPA are set that  $h=2$  mm,  $d=1.5$  mm and  $S=4$  mm, the three different  $D$  values are 20, 30 and 50 mm, and  $MCP_1 \sim MCP_6$  are corresponding to the six groups conductance sensors. After consulting the relevant literature and information, owing that the oil phase is considered as the non-conductive material and has

no conductive property, and the oil belongs to low-conductivity material. And it can be known from the water and oil conductive property that the water conductivity  $\sigma_w$  is greater than the oil–water mixture conductivity  $\sigma_m$ , and the  $\sigma_m$  is larger than the oil conductivity  $\sigma_o$ . Hence, in horizontal oil–water flow with high water cut, the response signals with the minimum amplitude, which can be considered as the water phase calibration signals, can be obtained by the bottom location of the cross section of MCPA insulated flow pipe, that is, the location of  $MCP_1$ .

Owing that the ratio of the oil–water contact interface height of MCPA insulated flow pipe cross-section  $H_w$  and the parameter  $D$  is  $H_w/D = (1 - \cos \alpha/2)/2$  and  $\alpha$  is the corresponding central angle, the range of the  $H_w/D$  is

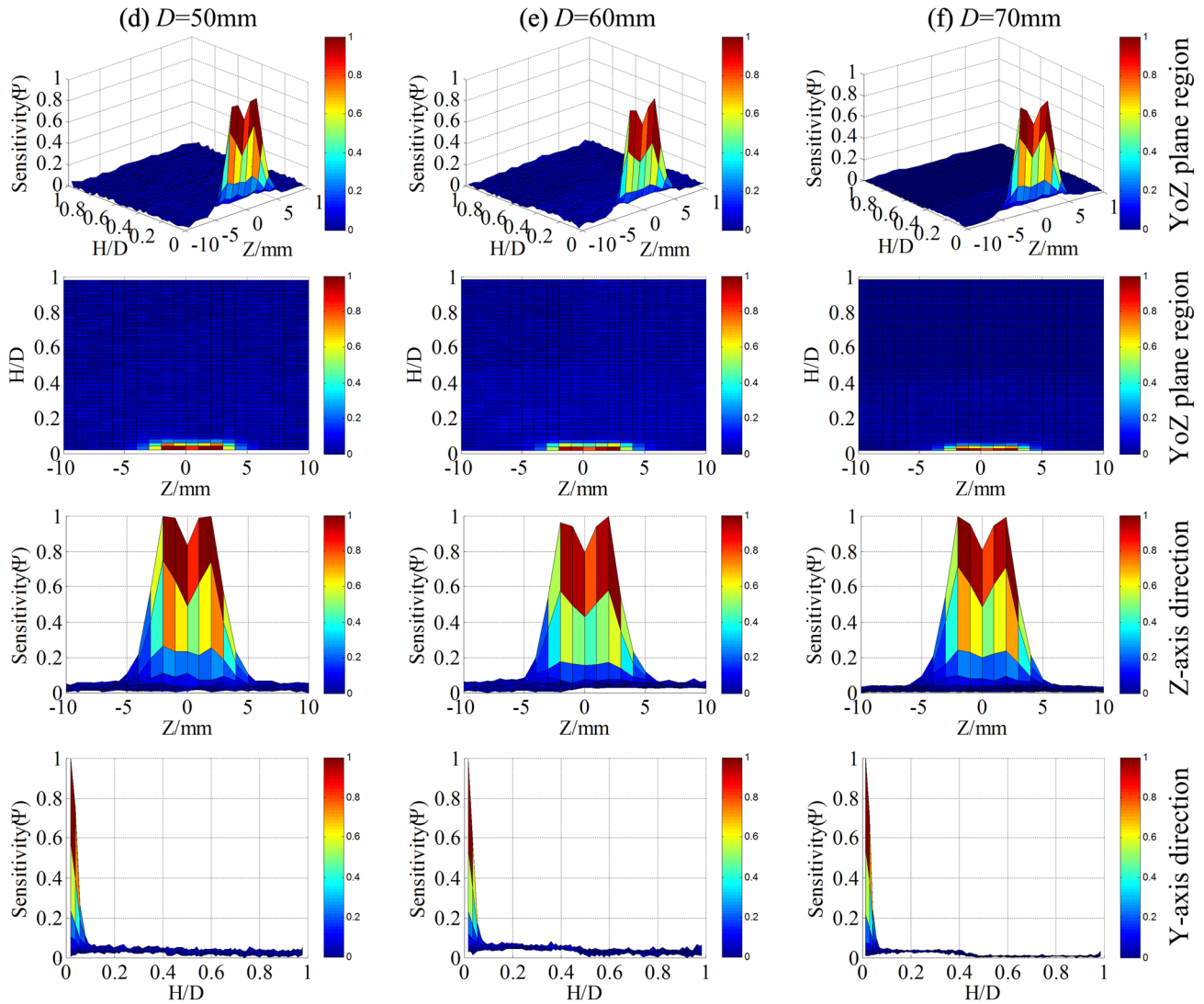


Fig. 7 (continued)

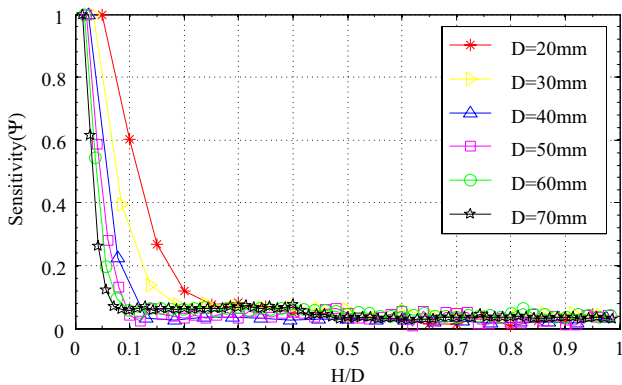


Fig. 8 Sensitivity distribution curves of MCP<sub>1</sub> under six different D values at z=0: h=2 mm, d=1.5 mm and S=4 mm

(0, 1). The relation between the water cut  $y_m$  and  $H_w/D$  is nonlinear. When  $y_m = 1$  or  $H_w/D = 1$ , the fluid in the insulated flow pipe shows a water phase; and when  $y_m = 0$  or  $H_w/D = 0$ , the fluid in the insulated flow pipe shows an oil phase. In addition, the fluid in the insulated flow pipe shows an oil–water mixture phase and the response values of the sensors are corresponding to the oil–water mixture conductivity under the condition that  $0 < y_m < 1$  or  $0 < H_w/D < 1$ .

### Experimental facility

In the practical process of the logging, using the voltage signals for long-distance transmission would cause the signals attenuation and severe distortion, while the frequency signals have the characteristics of the lower attenuation and



long-distance transmission. Simultaneously, in order to avoid the polarization phenomenon, the system adopted the alternating constant voltage source as the exciting signals. Figure 9 shows an operating principle of MCPA frequency measurement system, which consists of a 20 kHz sinusoidal exciting source with inhibit current loss, multiplex programmable analog switch circuit, signal amplification, filtering and demodulation circuit, RMS to DC converter,  $V/F$  conversion measurement circuit, sampling resistor, power supply, composite signal frequency measurement system and PC.

Figure 10a, b shows PCBs of MCPA frequency measurement system circuitry, and the system circuitry consists of conductance water cut meter multiplex excitation and control circuit using digital power supply drive as A board and multi-signal transmission circuit using analog power supply drive as B board. From Fig. 10, the A\_S-XWR&B\_LS-XWR series are specially designed for applications where a group of polar power supplies are isolated from the input power supply in a distributed power supply system on A circuit board. In order to inhibit current loss, we are now

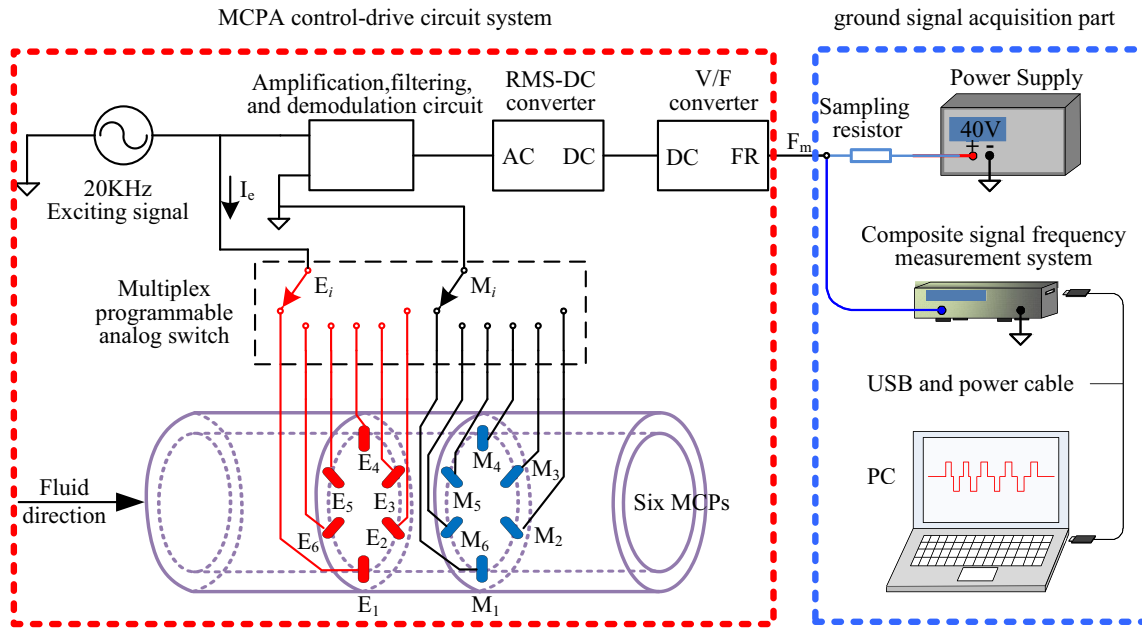


Fig. 9 Sketch of operating principle of MCPA frequency measurement system

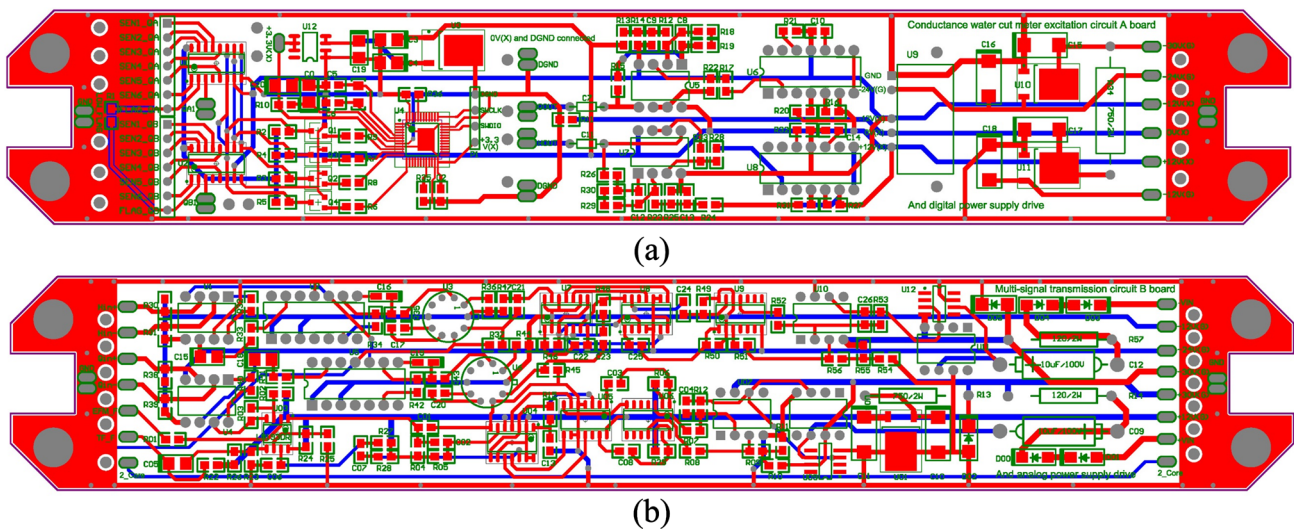


Fig. 10 PCBs of MCPA frequency measurement system circuitry: **a** conductance water cut meter excitation circuit A board using digital power supply drive, **b** multi-signal transmission circuit B board using analog power supply drive

taking a new scheme with the introduction of digital power supply and analog power supply isolation system using the A\_S-XWR&B\_LS-XWR series, and the integrated circuit constructed by ICL8038 and peripheral components as the 20 kHz sinusoidal exciting source with the introduction of digital power supply system, the integrated circuit constructed by AD620 and peripheral components as the differential operational amplifier, low-pass filter and signal demodulator with the analog power supply system to process the alternating current signal generated by the measuring electrodes, the integrated circuit AD637 as the RMS to DC converter, and the integrated circuit AD537 as V/F conversion measurement circuit to avoid the voltage loss on the long-distance transmission. And the integrated multiplex programmable analog switch circuit mainly consists of the microcontroller STM32FXXX series and single 8-channel analog multiplexer CD4051 using the introduction of digital power supply. All the electronic components involved in Fig. 10 are selected as military level. And the working temperature condition of the designed MCPA system prototype is in  $-55$ – $125^{\circ}\text{C}$  and the overall pressure resistance is 30 Mpa, meeting the downhole complex environment requirements of the high temperature and high pressure in the practical logging.

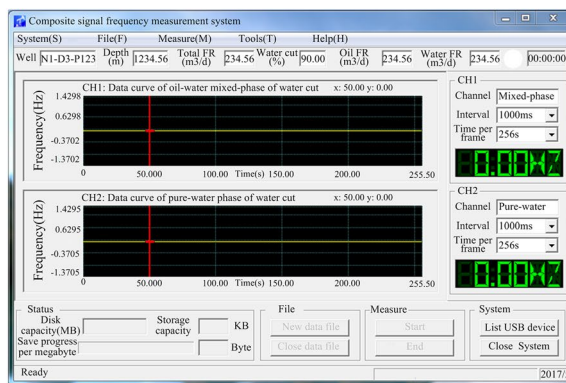
The data acquisition equipment is selected from the Yan-shan University's independent development product: the composite signal frequency measurement system, which is based on the USB 2.0 port. Equipped with three sampling channels and selector switch, the data processing part is implemented through graphical programming language software for MFC, which can make real-time frequency data waveform displaying, storing, reviewing and analyzing, as is shown in Fig. 11.

The instrument output is expressed by the frequency signal  $F_m$ (KHz) which can be described as:

$$F_m = k_m \times V_m \times 10^{-3} \quad (3)$$



(a)



(b)

**Fig. 11** Multi-channel signal frequency acquisition platform: **a** hardware of composite signal frequency measurement system, **b** software of composite signal frequency measurement system

where  $k_m$  is the correction coefficient of the linearity conversion,  $V_m$  is the output voltage of the measurement electrodes.

Figure 12 shows the photos of MCPA with three different inner diameters and the gold-plated electrode with  $h=2$  mm and  $d=1.5$  mm. The experimental media were tap water and industrial white oil. In the experiment, the fluid is forced into the insulated flow pipe of MCPA with  $D=20$  mm, 30 mm and 50 mm, respectively, from a large diameter horizontal plexiglass pipe. The response values of both the  $y_m$  and  $H_w/D$  can be obtained corresponding to the different flow conditions by changing the oil cut of the oil–water mixture.

## Static experiment

Figure 13 shows the frequency response curves with three different  $D$  values in horizontal segregated flow under different values of  $y_m$  and  $H_w/D$ , respectively. It can be seen from Fig. 13 with the increase in the  $y_m$  or  $H_w/D$ , the response value  $F_m$  of the MCP<sub>1</sub> with three different  $D$  values becomes small and tends to be the response values corresponding to the water conductivity. It can be known from Fig. 13a that the frequency response values of MCP<sub>1</sub> with three different  $D$  values is larger and the rate of change is fast when  $y_m < 5/D$  (when  $D=20$  mm,  $y_m < 0.25$ ), which shows that the sensors with different  $D$  values in that condition are seriously influenced by the oil phase. It can be also known that the frequency response values of MCP<sub>1</sub> with three different  $D$  values is relative stable and approximate to the response values corresponding to the water conductivity when  $y_m > 5/D$ , which shows that the sensors with different  $D$  values in that condition are hardly influenced by the oil phase and the response values obtained can be used as the calibrated values for the water phase. It can be known from Fig. 13b that the frequency response values of MCP<sub>1</sub> with three different  $D$  values is larger and the change rate is fast when  $H_w/D < 6/D$  (when



Fig. 12 Photos of MCPA with different  $D$  values and gold-plated electrode: **a**  $D=20$  mm, **b**  $D=30$  mm, **c**  $D=50$  mm, **d**  $h=2$  mm,  $d=1.5$  mm

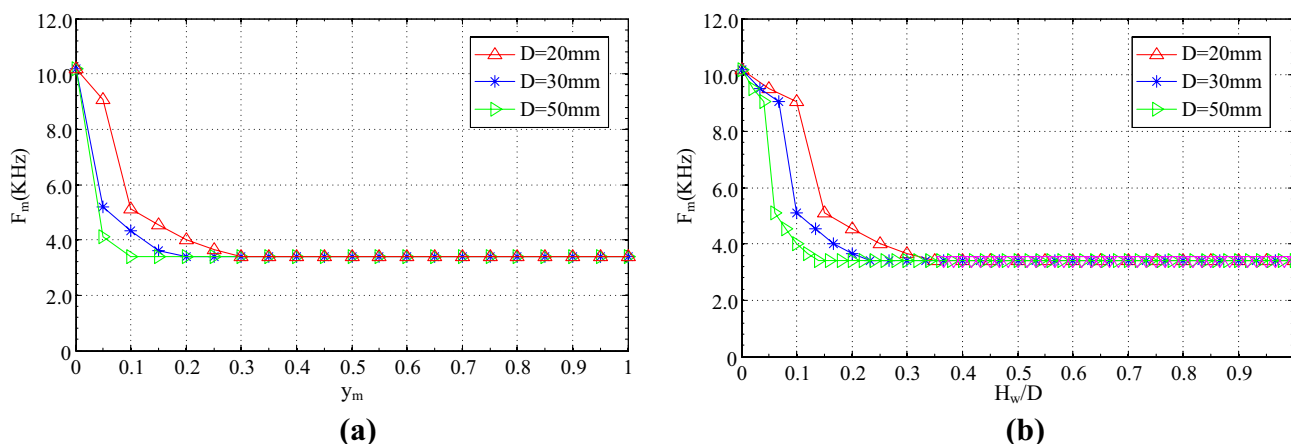


Fig. 13 Frequency response curves of  $MCP_1$  under different  $D$  values at horizontal segregated flow condition:  $h=2$  mm,  $d=1.3$  mm and  $S=4$  mm: **a**  $F_m$  versus  $y_m$ , **b**  $F_m$  versus  $H_w/D$

$D=20$  mm,  $H_w/D < 0.3$ ), which shows that the sensors with different  $D$  values in that condition are seriously influenced by the oil phase. It can be also known that the frequency response values of  $MCP_1$  with three different  $D$  values is relatively stable and approximate to the response values corresponding to the water conductivity when  $H_w/D > 6/D$ , which shows that the sensors with different  $D$  values in that condition are hardly influenced by the oil phase and the response values obtained can be used as the calibrated value for the water phase. And simultaneously, when  $D=50$  mm, the sensor can obtain a stable calibrated value corresponding to the water conductivity in the condition that  $y_m > 5/50$  or  $H_w/D > 6/50$ .

From the above analysis, when  $y_m > 5/D$  or  $H_w/D > 6/D$ , the response value of  $MCP_1$  with three different  $D$  values approximate to the measurement value

corresponding to the water conductivity. And simultaneously, with the increase in the inner diameter of the sensor, the critical point of the  $y_m$  where the sensors comes to the stable response values changes from  $5/20$  to  $5/50$  and the critical point of the  $H_w/D$  where the sensors comes to the stable response values changes from  $6/20$  to  $6/50$ .

### Experiment and analysis under different mineralization degree and temperature

In order to investigate the response characteristics for the different mineralization degree of water and temperature in the fluid to the three different inner diameters of MCPA and the corresponding linear relation between MCPA with different inner diameters and RSCP with ID = 20 mm, considering the high mineralization degree and high temperature in real oil-producing wells, the paper carried out the experiment

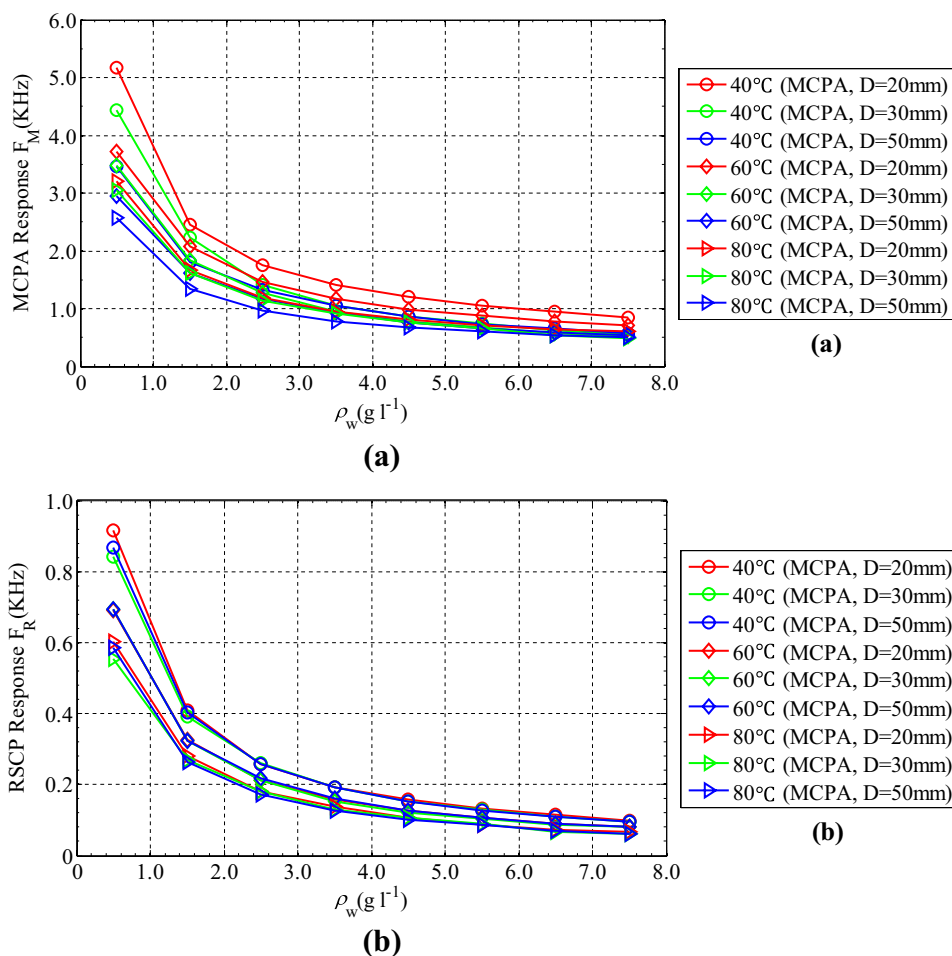
research on the different mineralization degree of water using three different inner diameters of MCPA and RSCP with high temperature in the simulation well experimental facility. When carrying out the routine mineralization degree calibration, the different values of water salinity  $\rho_w$  are used to represent the different mineralization degree of water and  $\rho_w = 1.0 \text{ g l}^{-1}$  represents the mineralization degree 1000 ppm. Hence, the response values of the experiment are calculated at the condition of filling with continuous water medium in the insulated pipe under different values of  $\rho_w$  in which the range of  $\rho_w$  is from  $0.5 \text{ g l}^{-1}$  to  $7.5 \text{ g l}^{-1}$ . Figure 14 shows the response values of between MCPA with different inner diameters and RSCP for water medium measurement in terms of different values of  $\rho_w$  and different temperature  $T_w$ , respectively, in horizontal pipe, where  $\rho_w$  is set to  $0.5 \text{ g l}^{-1}$ ,  $1.5 \text{ g l}^{-1}$ ,  $2.5 \text{ g l}^{-1}$ ,  $3.5 \text{ g l}^{-1}$ ,  $4.5 \text{ g l}^{-1}$ ,  $5.5 \text{ g l}^{-1}$ ,  $6.5 \text{ g l}^{-1}$ , and  $7.5 \text{ g l}^{-1}$ , and  $T_w$  is set to  $40^\circ$ ,  $60^\circ$ , and  $80^\circ$ , respectively. As can be observed from Fig. 14, under the same temperature condition, with the increase in  $\rho_w$ , the measured frequency results of MCPA with different inner diameters and RSCP show a decreasing tendency and obvious difference which can be attributed to the distinctive difference of  $\rho_w$ . Under the same mineralization degree condition, with the increase

in  $T_w$ , the measured frequency results of MCPA with different inner diameters and RSCP show a decreasing tendency and obvious difference which can be attributed to the distinctive difference of  $T_w$ . Meanwhile, the response values of MCPA with different inner diameters exhibit obvious difference. And the response values of the sensor with a larger inner diameter are relatively smaller, which is as a result that the difference in the sensor structure with different inner diameters makes a certain difference existed in the electric field of the corresponding excited electrodes.

According to Fig. 14, it can be observed that MCPA with different inner diameters and RSCP have nice response characteristics for water medium measurement under different values of  $\rho_w$  at different high temperatures, respectively. The current loss existed in the system circuits would exhibit a nonlinear change with the change of the fluid component or conductivity inside the sensors, causing the non-constant current in the measurement field of the sensors, which will lead to that the measurement results of MCPA with different inner diameters and RSCP show a nonlinear change under different values of  $\rho_w$  at different high temperatures.

Figure 15 shows the fitting curves of experiment results between MCPA with three different inner diameters and

**Fig. 14** Response values of conductance probes under different values of  $\rho_w$  at different high temperatures: **a** MCPA with  $D=20, 30$  and  $50$  mm, respectively, **b** RSCP with ID=20 mm





RSCP. As can be observed from Fig. 15, the abscissa positions corresponding to each discrete point with three different marker symbols represent the response values of RSCP experiment results, and the ordinate positions represent the response values of experiment results of MCPA with different inner diameters at the same condition with RSCP. The continuous curves represent relation curves of experiment results between MCPA with different inner diameters and RSCP by using the linear fitting. Under the same condition, the response values between MCPA with three different inner diameters and RSCP show a relatively nice linear function relation, and the relation curves can be given as:

$$\begin{cases} F_M = 5.1235F_R + 0.3218 & (\rho_w \in (0.5\text{g/L}, 7.0\text{g/L}), T_w \in (40^\circ\text{C}, 80^\circ\text{C}) \text{ and } D = 20 \text{ mm}) \\ F_M = 5.0391F_R + 0.1654 & (\rho_w \in (0.5\text{g/L}, 7.0\text{g/L}), T_w \in (40^\circ\text{C}, 80^\circ\text{C}) \text{ and } D = 30 \text{ mm}) \\ F_M = 3.8095F_R + 0.2821 & (\rho_w \in (0.5\text{g/L}, 7.0\text{g/L}), T_w \in (40^\circ\text{C}, 80^\circ\text{C}) \text{ and } D = 50 \text{ mm}) \end{cases} \quad (4)$$

where  $F_R$  is the measured frequency of RSCP,  $F_M$  is the measured frequency of MCPA and  $\rho_w$  is the water salinity.

The good and bad points of the fitting curves by the response values of MCPA with different inner diameters and RSCP in different mineralization degree and temperature conditions is measured by the relative index  $R^2$  of the curve fitting degree (Kong et al. 2016a). According to Eq. (4), the corresponding relative indexes of MCPA with three different inner diameters and RSCP fitting curves in different mineralization degree and temperature conditions can be obtained:

$$\begin{cases} R^2 = 1 - \frac{0.15715073}{28.65421296} = 0.9945 & (\rho_w \in (0.5 \text{ g/L}, 7.5 \text{ g/L}), T_w \in (40^\circ\text{C}, 80^\circ\text{C}) \text{ and } D = 20 \text{ mm}) \\ R^2 = 1 - \frac{0.12408175}{0.05699746} = 0.9949 & (\rho_w \in (0.5 \text{ g/L}, 7.5 \text{ g/L}), T_w \in (40^\circ\text{C}, 80^\circ\text{C}) \text{ and } D = 30 \text{ mm}) \\ R^2 = 1 - \frac{24.53771163}{14.81896733} = 0.9962 & (\rho_w \in (0.5 \text{ g/L}, 7.5 \text{ g/L}), T_w \in (40^\circ\text{C}, 80^\circ\text{C}) \text{ and } D = 50 \text{ mm}) \end{cases} \quad (5)$$

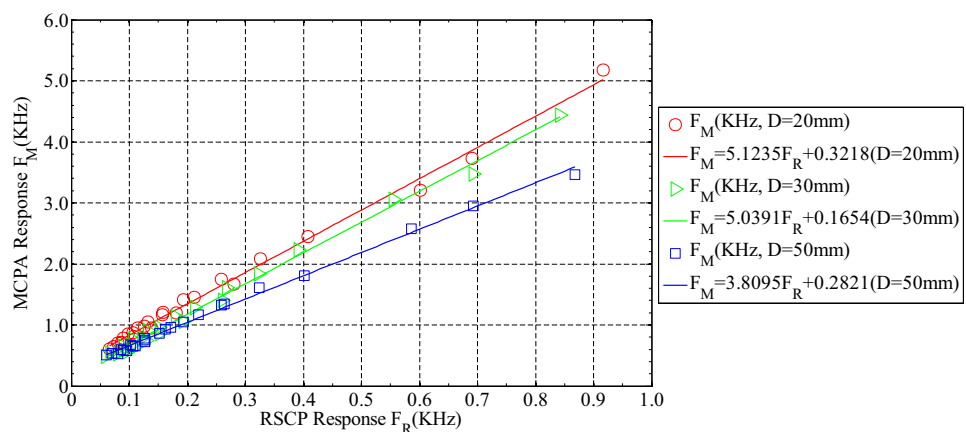
Analyzed from the relative index  $R^2$ , with the change of mineralization degree and temperature, the curve fitting degrees

are better, and MCPA with three different inner diameters and RSCP in different mineralization degree and conditions have a nice linear relation, hardly influenced by the mineralization degree and temperature. Consequently, MCPA with different inner diameters have a better characteristic and a linearly proportional relation in different mineralization degree and temperature, so it can meet the actual requirements with high mineralization degree water and high temperature of the oil-producing wells better. In the actual work, the response values obtained by MCPA with different inner diameters and the response values obtained by RSCP in the downhole are substituted directly into the interpretation chart of the relative conductivity and the

interpretation chart is obtained by the calibration in different flow rate and water cut conditions in the simulation well experimental facility using the MCPA- and RSCP-based instruments. And some errors would be generated by the current leakage and the influence of temperature on the system circuits for the linear fitting curves of MCPA and RSCP in different conditions of both  $\rho_w$  and  $T_w$ . Meanwhile, there exists some difference in the coefficient of the corresponding fitting curve, as a result of the different structure parameters of MCPA with different inner diameters and machining error, when the inner diameter

of MCPA values differently, and the corresponding curve has a nice fitting index.

**Fig. 15** Relation curves of experiment results with between MCPA with three different inner diameters and RSCP under the conditions of  $\rho_w \in (0.5 \text{ g l}^{-1}, 7.5 \text{ g l}^{-1})$  and  $T_w \in (40^\circ\text{C}, 80^\circ\text{C})$



## Conclusions

In consideration of the problem that the response values corresponding to the water conductivity cannot be obtained by RSCP for water holdup measurement in horizontal oil–water two-phase flow, the spatial sensitivity distribution of MCPA in the measurement field with different structure parameters  $S$  and  $D$  was discussed and analyzed, on the theoretical model foundation of MCPA for water conductivity measurement in horizontal segregated flow. And the optimum structure parameters of the sensors for segregated flow measurement are obtained, that is, when  $S=4$  mm, the spatial sensitivity is more uniform. The response characteristics of MCPA with different  $D$  values was analyzed by the simulation experiments, the spatial sensitivity distribution curve of which and the response values curve show a nice consistency. The experimental results verified that the response characteristics of MCPA with three different  $D$  values are basically consistent under different  $y_m$  or  $H_w/D$  and that the characteristic of MCPA is hardly influenced by the insulated oil phase or non-conductive materials under the condition that  $y_m > 5/D$  or  $H_w/D > 6/D$ . And it analyzed response characteristics and indicated good linearity characteristics between the designed MCPA with three different inner diameters and RSCP for pure-water phase measurement with experiments under different mineralization degrees of water and different temperatures. The experiment results of the sensors with three inner diameters in different flow rates show that the sensor with the inner diameter 50 mm is more suitable to the water cut measurement when the flow rate is large, and the reliable calibrated values corresponding to the water conductivity can then be obtained, which meets the demand of horizontal oil-producing wells.

**Acknowledgements** This research are supported by the National Science and Technology Major Project of the Ministry of Science and Technology of China, Grant number No. 2017ZX05019001-011; the Project funded by China Postdoctoral Science Foundation, Grant number No. 2018M631763; Yanshan University Doctoral Foundation, Grant number BL18010; and the Research of Yanshan University for Youths under Grant No. 15LGA009.

**Open Access** This article is distributed under the terms of the Creative Commons Attribution 4.0 International License (<http://creativecommons.org/licenses/by/4.0/>), which permits unrestricted use, distribution, and reproduction in any medium, provided you give appropriate credit to the original author(s) and the source, provide a link to the Creative Commons license, and indicate if changes were made.

## References

- Asali JC, Hanratty TJ, Andreussi P (1985) Interfacial drag and film height for vertical annular flow. *AIChE J* 31(6):895–902. <https://doi.org/10.1002/aic.690310604>
- Devia F, Fossa M (2003) Design and optimisation of impedance probes for void fraction measurements. *Flow Meas Instrum* 41(4):139–149. [https://doi.org/10.1016/s0955-5986\(03\)00019-0](https://doi.org/10.1016/s0955-5986(03)00019-0)
- Feng M, Yu HQ, Wen RH, Qin MJ, Chen Q, Duan YL (2018) Measurement scheme of water holdup based on resistance method. *Well Logging Technol* 42(1):1–7
- Gao HM, Xu ZL, Yu SM (2010) Sensitivity distribution of electrodynamic sensor array. *Proc Chin Soc Electr Eng* 30(5):76–82
- Guo HM, Liu JF, Dai JC, Wang K, Song HW (2009) Interpretation models and charts of production profiles in horizontal wells. *Sci China* 52(1):159–164. <https://doi.org/10.1007/s11430-009-5005-9>
- Jin ND, Xin Z, Wang J, Wang YZ, Jia XH, Chen WP (2008) Design and geometry optimization of a conductivity probe with a vertical multiple electrode array for measuring volume fraction and axial velocity of two-phase flow. *Meas Sci Technol* 19(4):045403–045421. <https://doi.org/10.1088/0957-0233/19/4/045403>
- Johansen G, Jackson P (2000) Salinity independent measurement of gas volume fraction in oil/gas/water pipe flows. *Appl Radiat Isot* 53(4):595–601. [https://doi.org/10.1016/s0969-8043\(00\)00232-3](https://doi.org/10.1016/s0969-8043(00)00232-3)
- Kong LF, Li L, Kong WH, Liu XB, Li YW, Zhang SL (2015) Overview of logging technique in oil production horizontal and high deviated well. *J Yanshan Univ* 39(1):1–8
- Kong WH, Kong LF, Li L, Liu XB (2016a) Calibration of mineralization degree for dynamic pure-water measurement in horizontal oil-water two-phase flow. *Meas Sci Rev* 16(4):218–227. <https://doi.org/10.1515/msr-2016-0027>
- Kong WH, Kong LF, Li L, Liu XB, Xie RH, Li J, Tang HT (2016b) The finite element analysis for a mini-conductance probe in horizontal oil-water two-phase flow. *Sensors* 16(9):1352. <https://doi.org/10.3390/s16091352>
- Kong WH, Kong LF, Li L, Liu XB, Cui T (2017) The influence on response of axial rotation of a six-group local-conductance probe in horizontal oil-water two-phase flow. *Meas Sci Technol* 28(6):065104–065125. <https://doi.org/10.1088/1361-6501/aa6708>
- Li H, Ji H, Huang Z, Wang B, Li H, Wu G (2016) A new void fraction measurement method for gas-liquid two-phase flow in small channels. *Sensors* 16(2):159–172. <https://doi.org/10.3390/s16020159>
- Lucas G, Cory J, Waterfall RC (2000) A six-electrode local probe for measuring solids velocity and volume fraction profiles in solids-water flows. *Meas Sci Technol* 11(11):1498. <https://doi.org/10.1088/0957-0233/11/10/311>
- Lum JYL, Alwahaibi T, Angeli P (2006) Upward and downward inclination oil-water flows. *Int J Multiph Flow* 32(4):413–435. <https://doi.org/10.1016/j.ijmultiphaseflow.2006.01.001>
- Oddie G, Pearson JRA (2004) Flow-rate measurement in two-phase flow. *Annu Rev Fluid Mech* 36(1):149–172. <https://doi.org/10.1146/annurev.fluid.36.050802.121935>
- Sætre C, Johansen GA, Tjugum SA (2010) Salinity and flow regime independent multiphase flow measurements. *Flow Meas Instrum* 21(4):454–461. <https://doi.org/10.1016/j.flowmeasinst.2010.06.002>
- Shi YY, Dong F, Tan C (2010) Characteristic of ring-shaped conductance sensor in two-phase flow measurement. *Proc Chin Soc Electr Eng* 30(17):62–66
- Trallero JL, Sarica C, Brill J (1996) A study of oil-water flow patterns in horizontal pipes. 1996 Offshore Technology Conference, Houston, the United States, pp 165–172
- Wang Z, Samanipour R, Kim K (2016) The cleanroom-free rapid fabrication of a liquid conductivity sensor for surface water quality monitoring. *Microsyst Technol* 22(9):2273–2278. <https://doi.org/10.1007/s00542-015-2544-1>
- Yang M, Wu XL, Wang ZL, Liu ZB, Huang ZJ, Wang JY, Peng WP, He FJ (2008) An experimental study of oil-water flow patterns in horizontal wells. *Well Logging Technol* 32(5):398–402. <https://doi.org/10.1007/s11442-008-0201-7>
- Zhai LS, Jin ND, Zheng XK, Xie RH (2012a) The analysis and modeling of measuring data acquired by using combination production logging tool in horizontal simulation well. *Chin J Geophys* 55(4):1411–1421. <https://doi.org/10.6038/j.issn.0001-5733.2012.04.037>

Zhai LS, Jin ND, Zong YB, Wang ZY, Gu M (2012b) The development of a conductance method for measuring liquid holdup in horizontal oil–water two-phase flows. *Meas Sci Technol* 23(2):025304–025318. <https://doi.org/10.1088/0957-0233/23/2/025304>

**Publisher's Note** Springer Nature remains neutral with regard to jurisdictional claims in published maps and institutional affiliations.